A Study of Radio Telescopes

at Three Centimeters and One Meter

Martin E. Zatzman

A Thesis

submitted in conformity with

the requirements for the degree of

Master of Science

in Saint Mary's University

© Martin E. Zatzman 1976

Department of Astronomy

Saint Mary's University

Halifax, N.S.

ACKNOWLEDGEMENTS

Table of Contents

CHAPTER I

INTRODUCTION

This thesis is the end result of the intial stages of
the radio astronomy program at Saint Mary's University.
The main objective of the project was to build a working
radio telescope and to test some important properties of
receiver systems for 3 centimeters and 1 meter. Also the
feasibility of a 3 centimeter and 1 meter interferometer
would be explored. The radio sun and its properties are
described in Chapter II. Chapter III discusses the basic
electronics and the development of the two receiver sys-
tems. Chapter IV describes the construction of a two-
element transit interferometer operating at 3 centimeters.
A discussion of sensitivity tests follows the construction
phases. The unexpectedly low solar flux at 3 centimeters
required that the effort of the thesis be turned to the
1 meter telescope system discussed in Chapter V, and this
was used for several weeks of observations. Finally,
Appendix C discusses the successful acquisition of fringes
with a prototype 1 meter solar interferometer.

Chapter II

The Radio Sun

This chapter will summarize the solar radio properties
that should be observable with the equipment available
or under developement at Saint Mary's University.

The radio spectrum extends from millimeter wavelengths
to meter wavelengths and is quite broad in comparison
to the visible spectrum. In Figure 2.1(Kraus ,1966),
solar flux densities are plotted verses two extremes, the
quiet sun and the active sun. The plot of flux density
versus wavelength shows the sun is much brighter at
centimeter wavelengths than at meter wavelengths. The
radiation at centimeter wavelengths originates close to the
photosphere and hence radio emission phenomena may be
correlated with optical data. The outer corona is opaque
to low frequency radiation and transparent to high
frequency radiation, hence at a given frequency the
radiation comes mostly from a layer located just above
the critical layer. The frequency of the critical layer
is a function of the square root of electron density.
The electron density of the solar atmosphere decreases
with height, so that the critical layer is close to the
photosphere at the highest frequencies, but is high in
the corona at the lower frequencies.

Figure 2.1

The solar spectrum from millimeter to meter wavelengths,
plotted versus the flux density. Two extremes are plotted
for the radio sun; the quiet sun and the active sun. This
diagram is adapted from (Kraus, 1966). The solar flux
density is equal to that from a blackbody radiator at
6000 ^{o}K at wavelengths less than 1 centimeter , but is
greater than this at longer wavelengths. At radio wave-
lengths the radiation is between that of quiet- and
active-sun curves. The straight lines give the flux density
corresponding to blackbody radiators at various tempera-
tures in degrees Kelvin.

Active sun

Quiet sun

10^{10} °K
10^9 °K
10^8 °K
10^7 °K
10^6 °K
10^5 °K
10^4 °K
6000 °K

WAVELENGTH, m

10^4
10^3
10^2
10
1
10^{-1}
10^{-2}
10^{-3}

FLUX DENSITY, W m^{-2} Hz^{-1}

10^{-18}
10^{-19}
10^{-20}
10^{-21}
10^{-22}
10^{-23}
10^{-24}
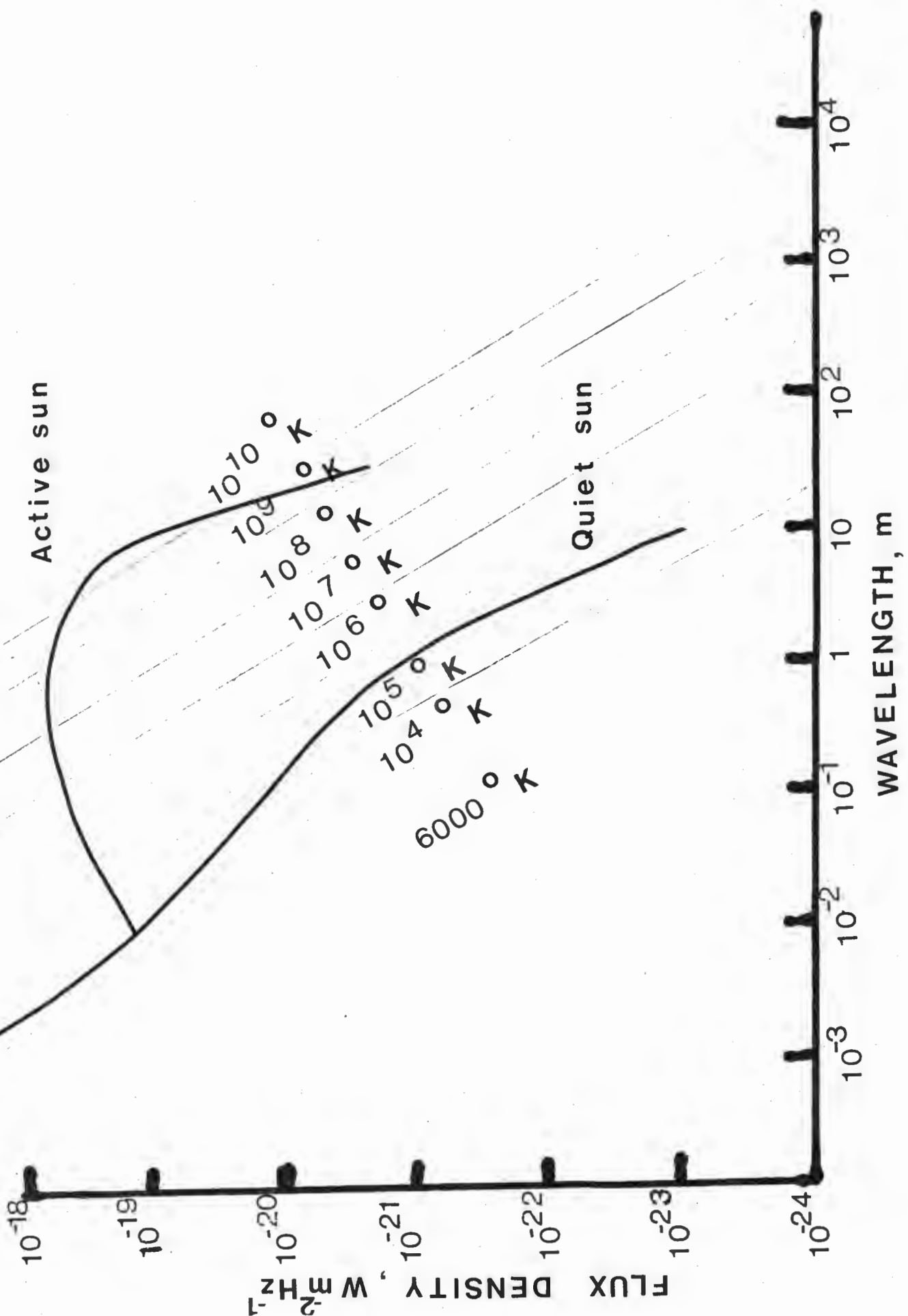
The slowly varying component (or S-Component) of solar emission shows fluctuations with a timescale of days, weeks, or even months and is observed from about 3 to 60 centimeters (Kraus, 1966). A correlation has been found between sunspot regions and the S-component, (Kakinuima and Swarup, 1962). The flux levels for the quiet sun average around 5×10^{-20} Watts meters^{-2} Hertz^{-1} at 3 centimeters and 1×10^{-22} W m^{-2} Hz^{-1} at 1 meter (Allen, 1973). When observing the sun on a detailed interferogram tracing, the sun will appear at its quiet level with superimposed S-component regions occuring on top of this level as illustrated in Figure 2.2 (Steinberg and Lequeux, 1963). Brightness temperature scans of the sun's disk are shown for about one month. The capability to distinguish the S-component depends on the resolution of the interferometer. For beams that are larger than the sun's radio disk, the S-component will not appear. However, beams of the order of minutes of arc will resolve these regions as an intensity maximum on the quiet sun level, as with the 3 cm interferometer discussed in this thesis. (Numbers on the disk refer to day of observation). On day one the emission was observed to come from the limb of the sun, while on day seven, it is seen near the center and on day fifteen, it is on the opposite limb of the sun, carried by the sun's rotation.

The variation in brightness temperature at several wavelengths is shown in Figures 2.3 and 2.4 (Gibson, 1973).

Figure 2.2

Brightness temperature scans taken with the Nançay
interferometer with a resolution of about four minutes of
arc. The lower envelope represents the contribution from
the quiet sun with the S-component occuring on top of
this level as followed at two day intervals. The figure
is adapted from Steinberg and Lequeux (1963). The size
of the visible disk is illustrated in comparison to the
radio disk at 3 centimeters.

quiet sun level

visible disk
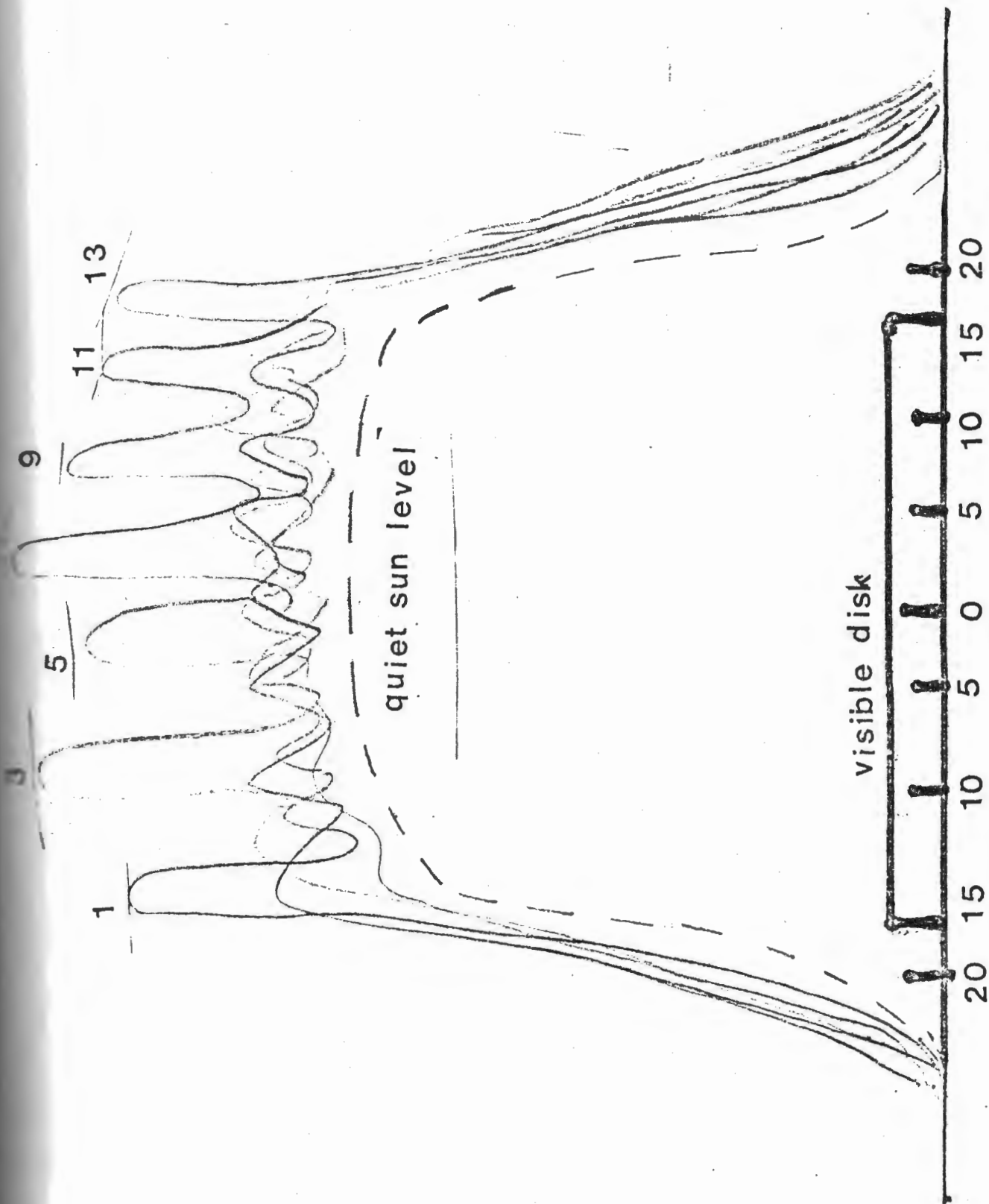
σ (arc minutes)

(The brightness temperature of any body is the temperature of a blackbody which would have the same monochromatic brightness at the frequency of observation.) Three effects are noticeable from Figures 2.3 and 2.4. First, as the wavelength increases to approximately two meters, the brightness temperature increases and limb brightening becomes pronounced. Secondly, as the wavelength increases beyond two meters, the brightness temperature decreases and a transition from limb brightening to limb darkening occurs. Finally, as the wavelength increases, the sun becomes larger and less well defined, regardless of optical thickness of the source . Because the source is both optically thick and located higher in the atmosphere, at longer wavelenghts the increase in brightness temperature and limb brightening result from the positive temperature gradient. Beyond two meters , the decrease in brightness temperature is the result of the optical depth decreasing to values much less than unity. Even though the temperature increases with height in the atmosphere, the net result is a decrease in total emission of radiation. The sun is the strongest radio source in our sky, and because of the continuously changing radio emission, it is an intriguing object for observations.

Figure 2.3

Brightness temperature calculated as a function of

R/R$_{sun}$ at several wavelengths. This diagram is

adapted from Gibson, 1973.

1cm

visible disk

75 cm

50 cm

25 cm

10cm

R/R_{sun}
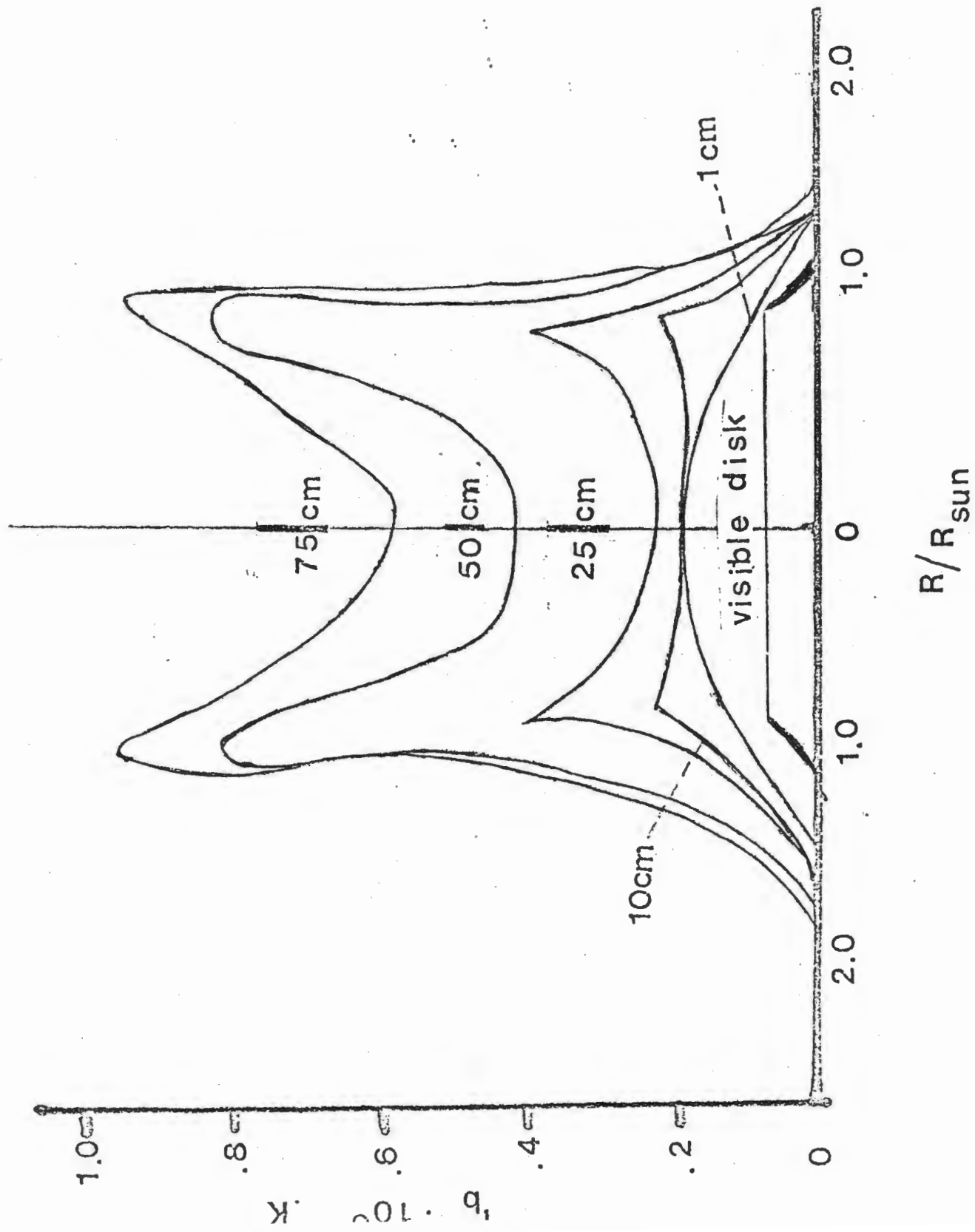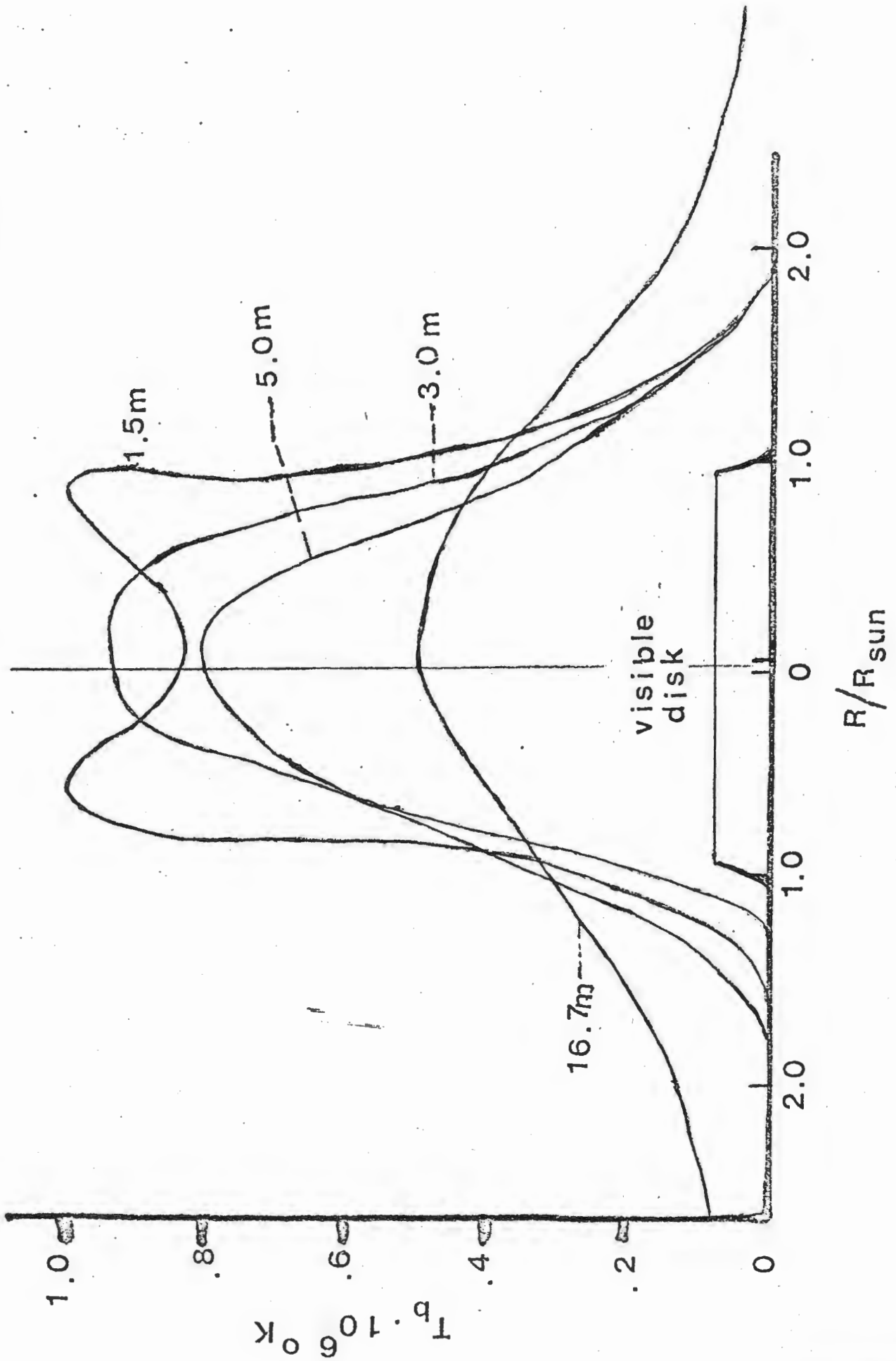
2.0   1.0   0   1.0   2.0

$T_b \cdot 10^6$ K

1.0   .8   .6   .4   .2   0

Figure 2.4

Brightness temperature calculated as a function of R/R_{sun} at several wavelengths. Adapted from Gibson, 1973.

Figure: Brightness temperature $T_b \cdot 10^6\,^\circ K$ as a function of R/R_{sun} for wavelengths 1.5m, 5.0m, 3.0m, and 16.7m, showing the visible disk.

Chapter III

Basic Electronics

The electronics used for both the 3 centimeter project and the 1 meter project employed similar techniques of design. The 1 meter electronics, however , had the added radio frequency(RF) pre-amplifier stage as is illustrated in Figure 3.1 by the broken lines.

From the antennas the 3 cm signal propagates up two approximately equal lengths of x-band waveguide to a receiver located midway between the two antennas. The signals from the two antennas are combined in a series tee-junction. A phase shifter was put into one line of the interferometer waveguide. The reason for doing this is to conveniently shift the main lobe in the beam pattern to the desired position so that it coincides with the axis of symmetry of the telescope. In other words,at transit it should appear that we have maximum constructive interference from the sun. If the main lobe has been shifted via the phase shifter to coincide with the axis of symmetry, this will occur. The phase shifter operates as follows: a dielectric wedge is inserted into the waveguide, and depending on the dielectric constant of the wedge and insertion depth, the propagation velocity of the wave is altered, hence the phase is shifted.

The receiver for both telescopes consisted of five main components: (1) the local oscillator;(2) the mixer;

(3) the intermediate frequency amplifier; (4) the
demodulation circuit; and (5) the final output direct
current (DC) amplifier and chart recorder. A block
diagram of the receiver is shown in Figure 3.1.

The signal voltage enters the mixing stage along
with a local oscillator voltage . The process is called
superhetrodyning and involves mixing the input RF signal
with a frequency of the same order of magnitude from the
local oscillator. One of the resultant voltages after
mixing will have a frequency suitable for amplification
in the IF stages.

Once the signal is amplified by the IF amplifier, it
is still not suitable for driving a chart recorder
directly because the signal oscillates between positive
and negative voltages with a mean value at zero. By using
a simple diode detector, suitably connected, the negative
voltage excursions are clipped while the positive
voltages are retained at full amplitude; therefore the
measured mean value of voltage is no longer zero, but
has some positive value.

The next stage of signal processing involves the DC
amplification stage. The amplifier produces a DC output
signal in response to a DC input. Direct current
amplifiers are required when DC and very-low-frequency
signals must be amplified as is the case here. At this
stage , it is useful to discuss the noise in the system.

The types of noise are the solar and the random noise. The solar noise here is that part which we are trying to record on the chart paper. A problem exists, however, due to the random noise, resulting from external noise radiation, antenna system noise, or noise generated within the receiver itself. One cause of noise is thermal agitation caused by the random movement of electrons (DeFrance, 1966). This random movement of current through a resistor causes a random noise voltage V (V=IR, where I=current and R=resistance). As the temperature of the component is increased, the thermal agitation is increased and the noise voltage is increased. The noise effect, however, is distributed throughout the radio frequency spectrum, and so the amount of noise in the receiver is also dependent on the receiver's bandwidth. Expressed as the Nyquist formula: $E_n = \sqrt{4 \times K \times T \times R \times BW}$ where E_n = the effective value of the noise voltage due to thermal agitation.

K= Boltzmann's constant

T= the absolute temperature

R= the resistance of the component

BW= the receiver bandwidth

An ideal receiver will always have only that noise predicated by Nyquist. In comparing the performance of receivers with respect to noise , the term noise figure (NF) is used. The figure compares the ratio of the signal power to the noise power at the input (S_i/N_i), to the

signal-to-noise power ratio at the output (S_o/N_o) (DeFrance, 1966).

$$NF = \frac{(S_1/N_1)}{(S_o/N_o)}$$

An ideal receiver (one that generates no noise) would have a noise figure of unity or 0 db.

This random noise generated by the receiver will than show up as a deflection on the chart paper. When the antenna is turned to a source generating a signal which is only a fraction of the receiver noise, it will not be detected because it will be only a slight increment superimposed on the receiver noise. The referance level background noise may be shifted from the receiver by putting in a DC offset voltage of opposite polarity and amplifying the difference (which will be the small increment) through the DC amplifier (Wolf, 1973). The final output voltage, appearing on the chart recorder is some function of the signal voltage.

The electronics were assembled from available University supplies and mounted in watertight aluminum boxes to insure long life and temperature stability of the system. If the temperature of the receiver is not kept constant, a resultant voltage drift would occur at the output of the chart recroder. As a result, the background noise level on the recorder showed considerabl

drift. Future receivers should incorporate a temperature controller to alleviate this problem.

Figure 3.1

Block diagram of a typical receiver package.
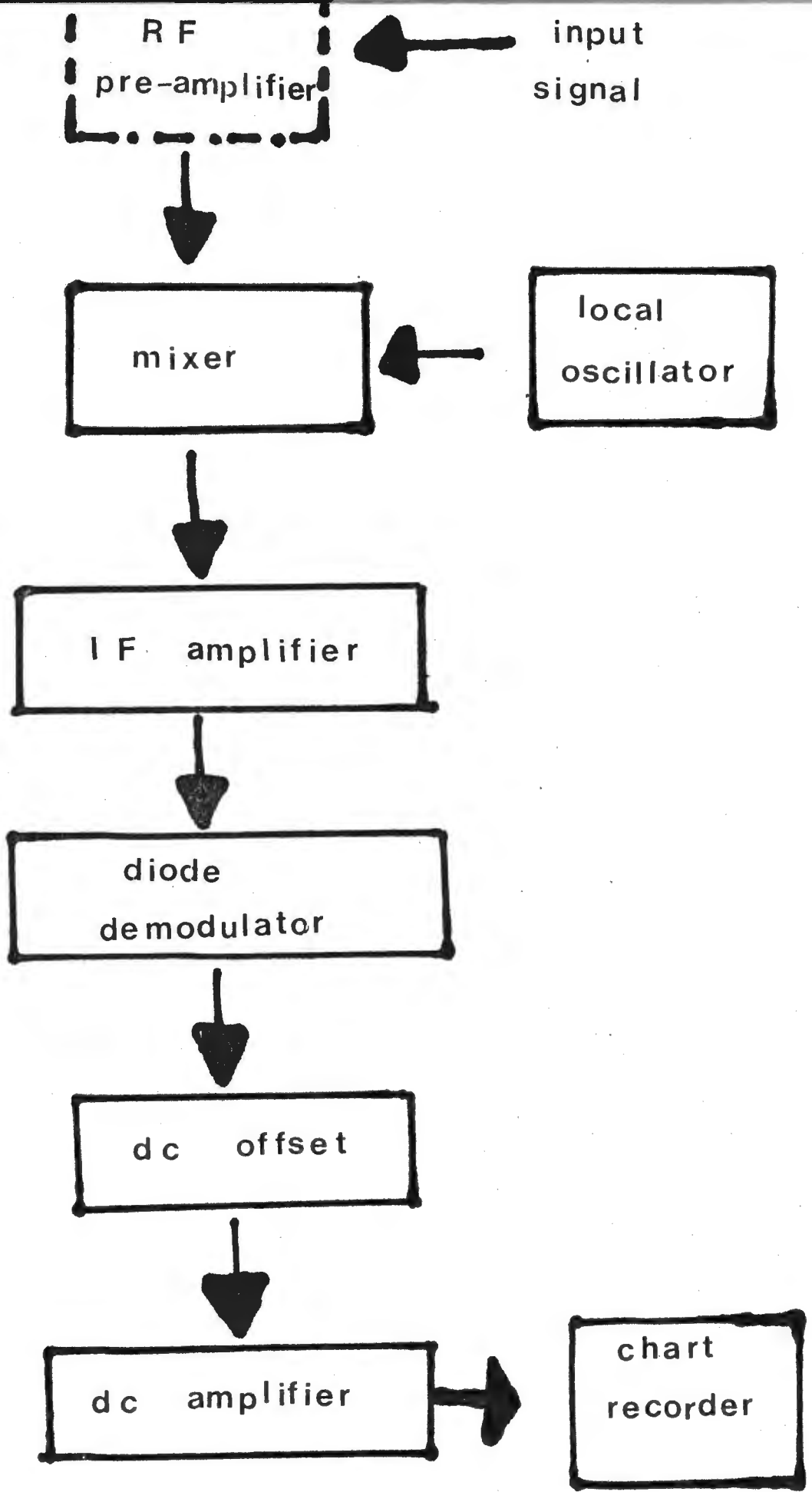
Chapter IV

The Three Centimeter Telescope

This chapter deals with the design, construction and sensitivity measurements used to build the two-element interferometer on the north wing of the main administration building at the University.

4.1 Construction

The two - element transit interferometer may be separated into two components: (1) the antennas and (2) the supporting structures associated with the antennas.

The Antennas: The antennas used for this project were sheet metal paraboloids operating at 10,000 MHz, salvaged from a telephone microwave relay system. The paraboloids are 2.44m in diameter, with the focus occuring at 95cm along the optical axis. The feed system support was constructed from three angle iron(dexion) braces and fastened to the paraboloid periphery. Two of the braces for the feed were positioned 180° apart, with the third brace spaced half - way in between the other two, for maximum support.

The feed itself was a small horn with flexible x-band waveguide connecting it to solid x-band guide which led out through the center of the antenna to the receiver package ,placed midway between the two antennas.

Supporting_Structures: The supporting structures for these antennas were designed in A-frame shapes. Two wooden frames were built for each antenna. The dimensions were 3.5m on each side of the equilateral triangular A-frame. The height of the structure was 3.05m . This allowed the 2.44m antennas to be supported with a freely rotating axis. The axis of rotation was made from 10cm steel pipe supported by bearings at each A-frame. The antennas were fitted with a rectangular back plate made of 2x6 inch wood. Then steel plates were bolted to the back frame of the antennas with U-bolts.

To achieve the desired declination, a lead screw was attached to each antenna and to an aluminum beam bolted across the back of the A-frames. Once each of the antennas were finished, they were rolled into place on the north wing of the administration building to form a 16.8m baseline. A series of 1.5m square boxes were then built and securely fastened, end to end , from one frame to the other. A catwalk was then laid down and the waveguide from each antenna to the receiver package, installed on that catwalk. To prevent the least amount of motion, a framework of wood was extended to the parapet walls of the roof perpendicular to the baseline. This would prevent the baseline from moving any significant distance. The entire interferometer may be seen in Plate I.

Plate I

3cm interferometer located on an East-West baseline
on the roof at Saint Mary's University.

The alignment of the two-element interferometer on
an East-West baseline was needed. With the use of a
transit an approximate E-W line was established.The
antennas were then positioned on this line. If the
antennas were out of position on the baseline the transit
of a celestial object would occur off the meridian. The
North-South alignment was also important since an error
on this axis would also cause the interference maxima
and minima of the pattern to occur at unexpected times.

A declination scale was constructed of plywood and
calibrated to within $\pm$ 0.30° by use of a plywood wedge
and a spirit level. The required pointing accuracy for
a wavelength of 3cm and antennas of 16.8m separation is
about $\pm$ 9 minutes of arc. Therefore some type of optical
alignment system is needed, with the required accuracy
to insure both antennas are pointed at the same co-ordinate
in space.

4.2 Sensitivity Measurements

One important goal in building a radio telescope is
to achieve adequate sensitivity. For the 3cm inter-
ferometer a sensitivity was required to enable observations
of the quiet sun.

First it will be useful to describe the theory used
in the discussion of this chapter. The general formula
used to determine the power present at the antenna feed
is P=ΔBAS.

P= the total received power in watts.

ΔB= the bandpass of the receiver in Hz.

A= the collecting area of the antenna in m^2.

S= the flux density of the source in $Wm^{-2}Hz^{-1}$.

In testing the receiver, the available power from the quiet sun at 3cm was calculated based on average flux density(Allen,1973). A 35% efficiency of the antenna and a 50% efficiency for the polarization of the feed were assumed(Silver,1964). Hence the final power expected from the sun was:

$$P = \triangle BAS \times \text{ efficiency}$$

The bandpass ($\triangle B$) of the receiver is 3.6 MHz, as may be seen in Plate II. The collecting area(A) was $4.6m^2$ and the flux density assumed was $5 \times 10^{-20} Wm^{-2}Hz^{-1}$(Allen, 1973). Therefore, the expected power is P= 1.6×10^{-13}W.

Since the 3cm signal generator was calibrated in dbm (decibels referenced to one milliwatt), a conversion to dbm is made, for P=1.6×10^{-10}mw. The general form of the conversion is:

$$db = 10\log \frac{P_{out}}{P_{in}} = 10\log \frac{(1.6 \times 10^{-10})}{(1 \text{ mw})} = -98 \text{dbm}.$$

Expressing the signal in microvolts we use $V=\sqrt{PR}$, where R is the impedance of the line (50 ohms) :

$\therefore V=\sqrt{PR} = 2.8 \mu V$.

The losses in the waveguide amounted to about 2db for each line. The expected losses are 0.5db/line(Adam,1969). The added 1.5db/line was probably due mainly to dirt and water that would attenuate the signal. This loss

Plate II

Sweep generator test done on the 3cm receiver using the
HP 8601-A Generator/Sweeper with a Tektronix Type
RM503 oscilloscope. The grids on the plate are $1cm^2$.
The curve is a plot of receiver response versus frequency,
which determines the bandpass at half-power.
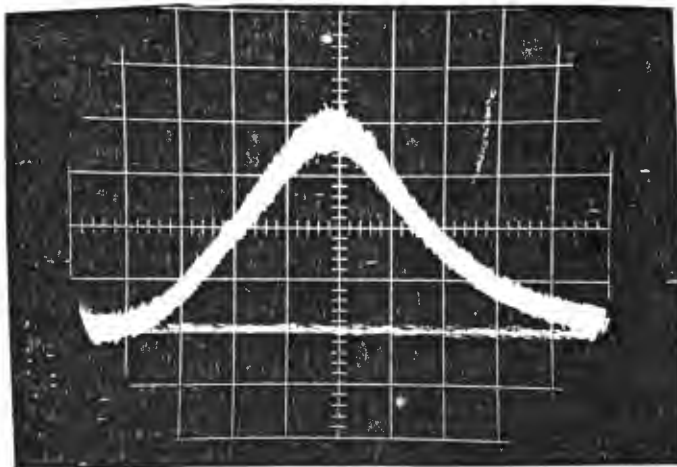
CALIBRATION — 1 MHz/cm

BANDPASS — 3.6 MHz

could be lowered by cleaning the waveguide, coating it
with silver or filling the waveguide with an inert gas,
but these were not feasible at the time of this project.
Hence to detect the sun at 3 cm with these antennas, the
receiver had to be sensitive to -100dbm. (This assumes a
nominal solar flux of $5 \times 10^{-20} Wm^{-2} Hz^{-1}$ and the antenna
efficiency of 35% in addition to the 50% loss in gain due
to polarization of the feed).

At this point in the project a series of tests were used
to further evaluate the sensitivity of the system as a
whole. The first test involved gain comparison with a
smaller antenna to see if the 2.44m antenna had the ex-
pected advantage over a 0.6m antenna. The 0.6m antenna
was a military quality paraboloid with installed dipole
feed and reflector of high quality so that a relatively
high efficiency was assumed. Installation of the 3 cm
feed horn had raised some doubts about the efficiency of
the larger antenna. To perform the test, a calibrated
attenuator (0 to 30 db) was connected to the output of a
test generator (TS-738A/UPM-11A). The attenuator was set
to 0db for the small antenna at a known distance R=32m.
A reading of 10 units was recorded on a simple receiver
consisting of a crystal detector and meter. The generator
was then pointed to the larger antenna at the same distance
and the attenuator was adjusted to achieve the same reading

of 10 units at the crystal detector. The gain was recorded
as 8db over the smaller antenna, compared to an expected
gain of 12db based on the collecting areas of the antennas.
Therefore it was established that a 4db loss was associated
with :   (1) the imperfections in the parabolic surface,
and/or   (2) the alignment of the feed on the geometrical
axis of the antenna. Most of the loss was probably due to
the feed alignment problems. At 3 cm the alignment was
found to be very critical. The theoretically calculated
tolerance for feeds of this wavelength is about 1 cm along
the geometrical axis, for the change in efficiency of the
antenna to be 50% (Silver, 1964, Christiansen and Hogbom,
1969). Therefore, adjustment of the feed at the focus was
found to be a major task. Another factor which contributes
to loss in gain is the feed tilt, with respect to the geo-
metrical axis. A feed tilt of 7 beamwidths gives a loss
in gain of 50%, or 3 db (Silver, 1964). In the case of the
antenna and wavelength used here, the beam is 42 minutes
of arc, hence a tilt of only 4.2 degrees would give a 3 db
loss.

A second experiment involved a laboratory demonstration
of the dilution of radiation from one horn as seen by
the second horn some distance away. This dilution is
an important step in evaluating the sensitivity of the
entire system. The HP-430B power meter and bolometer
were used as measuring devices. The results are shown

plotted in Figure 4.1. The data were fitted with a
least squares power law and the results for the exponent
were 2.01 $\pm$ 0.05. The error in measuring the power was
$\pm$ 0.01mw and this is the major contribution in the
exponent error of 0.05. Therefore,it is concluded
that the radiation falls off as an inverse square power
relation with distance. By placing the signal generator
(TS-147B/UP; calibrated from -40 to -85dbm) at a known
distance from the antenna, and by knowing the dilution
of radiation, a flux equivalent to that of the sun may
be simulated. The gain of the small antenna used for
this experiment was a factor of 21db above the small horn
used in the laboratory dilution experiment. Hence by
using the dilution factor based on the inverse square
law, then subtracting the gain introduced because of
the different collecting areas of the antenna and horn,
we may assess the losses incured over that distance. The
generator may then be set at a desired calibrated output
to simulate the flux of the sun. For example, for a
distance of 6.45m the expected dilution from the signal
generator and horn will be -48db. The gain of the small
radar antenna over the horn is 21db. Therefore the
dilution factor for that distance will be -27db. By
setting the dilution factor level, the solar flux may
be simulated. This information was used later to test

Figure 4.1

The inverse r^2 law, used to calculate the dilution
of radiation over a distance of known separation.

measuring
uncertainty in power
± 0.01 mw
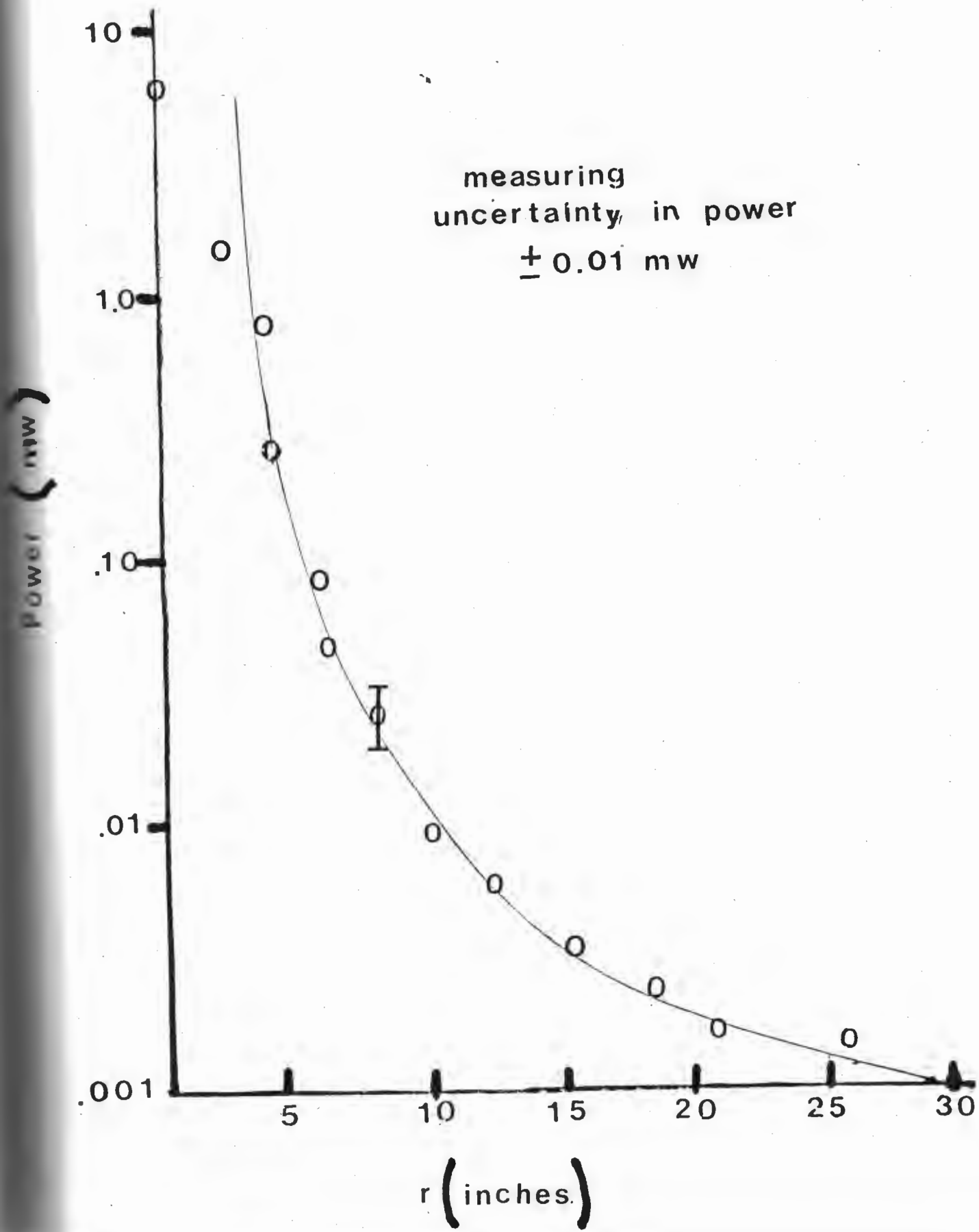
the antenna/receiver system with flux equivalent to that
of the sun.

Finally, recent solar flux measurements were obtained from
the Herzberg Institute of the National Research Council
in Ottawa. At the time those measurements were made (week
of June 1, 1976) the solar flux was about 66 solar flux
units (S.F.U.) at cm wavelengths. (One S.F.U. is equal
to $10^{-22} Wm^{-2} Hz^{-1}$). All power calculations had been based
on 500 S.F.U. Therefore for a level of 66 S.F.U. the
level of power would be down another factor of 8db.
Hence from the original power calculations and taking into
account the present solar flux, the power expected at
the receiver would be -108 dbm.

In conclusion, the present level of the quiet sun pro-
duces -108 dbm with this antenna system. Our available
equipment was sensitive to -107 dbm. Although the normal
quiet sun radiation would be detectable with this system,
the 66 S.F.U. radiation would be marginally detectable
with the equipment at hand. Two factors will enable
future observations : (a) the solar flux will increase
steadily, and (b) new low-noise receivers can be built,
using a Dicke switch or a low-noise mixer.

Chapter V

The One Meter Telescope

The next project was to study the sun at a longer wavelength. This chapter gives a brief outline of the construction of the one meter telescope along with sensitivity experiments performed on the receiver system that led to the detection of a signal from the sun. The last section discusses the method of observation and data reduction used.

5.1 Construction

The one meter radio telescope was built using a 2.44m parabolic antenna mounted with the one meter dipole as may be seen in Plate III. The antenna was mounted on a rectangular wooden frame and bolted on to an altitude-azimuth mounting on the roof at the University. The electronics package, Plate IV, was mounted in weather-tight boxes which were placed on the pedestal with the paraboloid as may be seen from Plate V. The platform on which the pedestal was mounted was stabilized with heavy wooden beams and the telescope pedestal itself was mounted on two steel beams.

5.2 Sensitivity Measurements

In the process of studying the 1m system several sensitivity tests were carried out. First, the expected power was calculated. The receiver had an IF bandwidth

Plate III

Alitude-Azimuth mounted one meter radio telescope with dipole feed at the focus of the antenna. The metallic rod above the dipole feed is called the reflector. It is used to increase the gain of the antenna.

Plate IV

The one meter electronics package is shown containing

the converter unit(combined mixer and local oscillator)

in the upper right. This is Vanguard Labs Model 407A

modified for 60 MHz IF. In the middle of the photo is

the RF pre-amplifier. This is Danel Labs Model PB with a

gain of 18db and a noise figure less than 3db. At the

bottom right is the demodulator circuit. The four sections
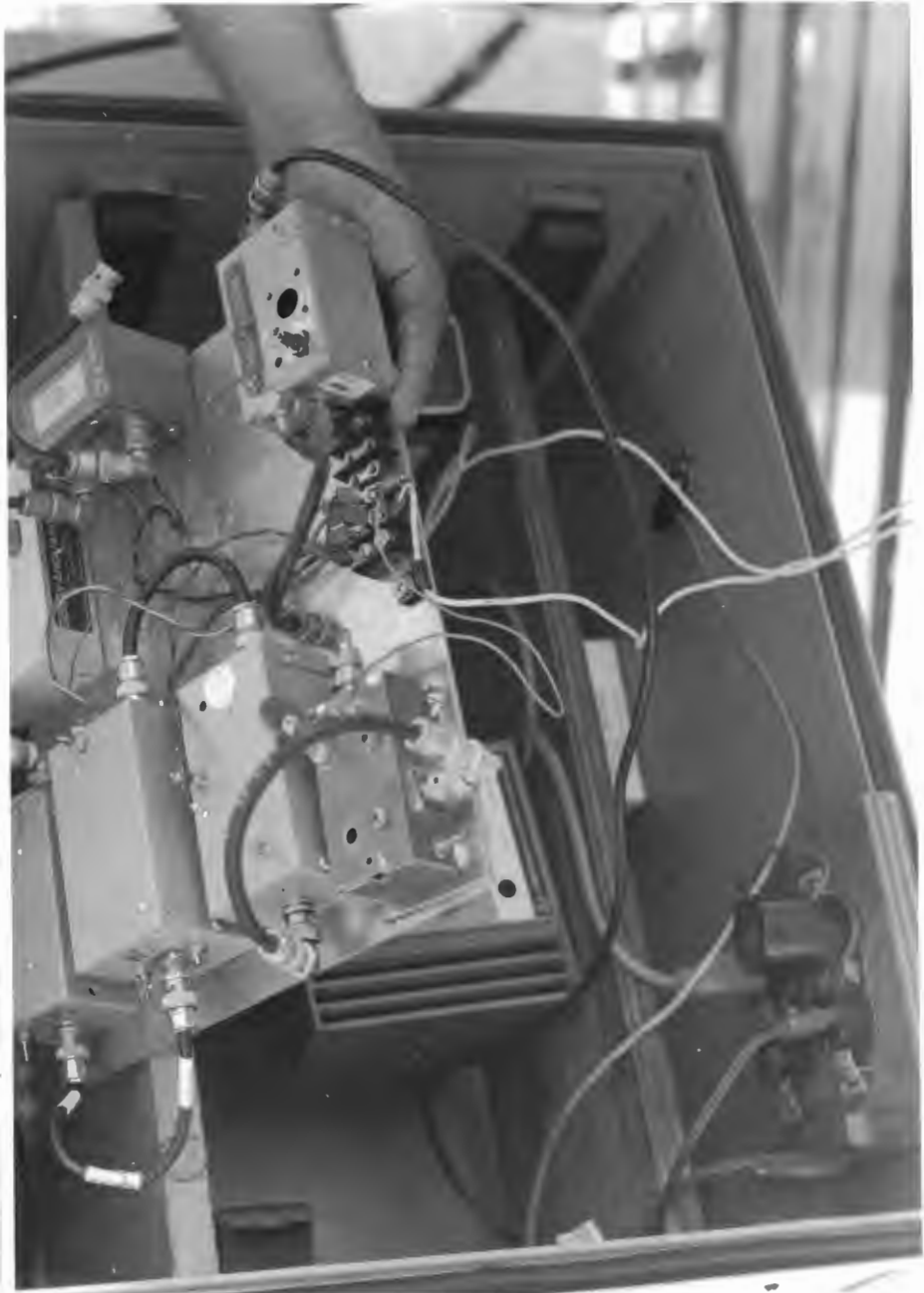
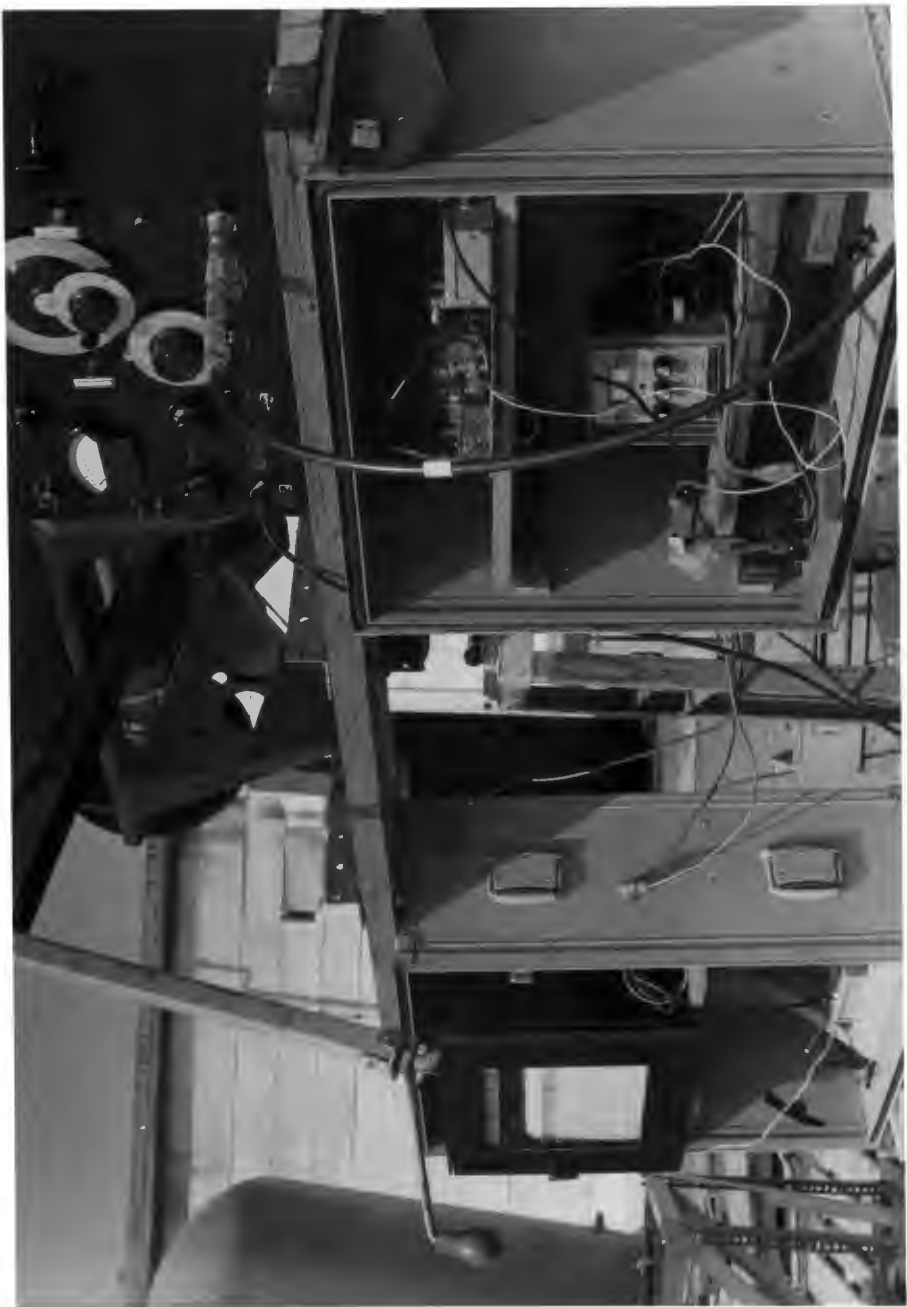of IF amplification appear on the left of the package.

Plate V

One meter electronics showing the chart recorder in the
left box at the top with the DC offset at the bottom.On
the right hand side we see the receiver section,while on
the top reclines the signal generator.

of $\triangle B=3MHz$, derived from the sweep signal shown in Plate VI. The area of the antenna is $4.6m^2$ and the nominal flux density from the quiet sun is approximately $1\times10^{-22}Wm^{-2}Hz^{-1}$(Allen,1973). Therefore the expected power is $P=2.4\times10^{-16}W$, which is -126dbm or $.10\mu V$.(We assume here a 50% efficiency due to the polarization of the feed and a 35% efficiency of the antenna.)

The first sensitivity test performed was to simply connect a signal generator(Type 1021-A,General Radio Company) to determine the minimal detectable signal level on the chart recorder. The receiver was found to be sensitive to $.08\mu V$ for a detectable deflection on the chart recorder. All sweep tests were performed with the Telonic 1205-Sweep Generator and Tektronix Type RM503 oscilloscope.

The dipole feed of the antenna was then connected to the receiver package and the one meter solar signal was acquired. An observing run was initiated to record daily radio emission from the sun at one meter.

5.3 Observations

The observations took place over a two week period at the end of June,1976. First a beam pattern was plotted with the telescope. This was done by moving the telescope through the sun by small increments in azimuth. The intensity (in arbitrary units normalized to one) was

Plate VI

One meter receiver sweep test using Telonic Model 1205
sweep generator in combination with Tektronix Type RM 503
oscilloscope. The grid is 1 cm^2 . The curve is a plot of
receiver response verses frequency and allows the measure-
ment of the bandpass at half power. The marker shows the
frequency of the maximum response of the receiver(253 MHz).

MARKER
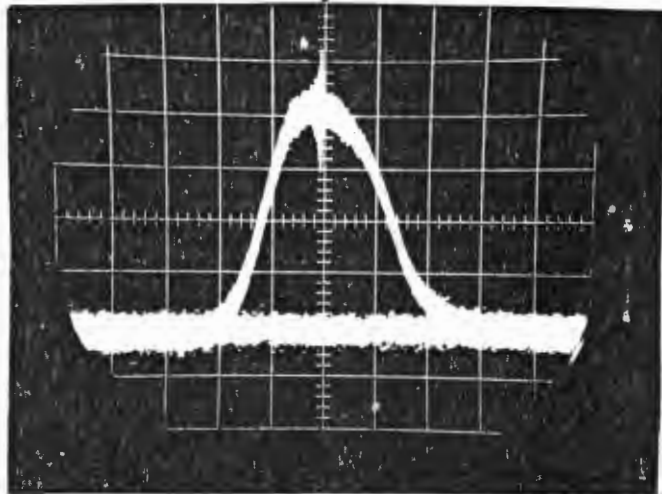
CALIBRATION   1.2 MHz/cm

BANDPASS   3 MHz

plotted verses azimuthal angle. The theoretical resolution or Half Power Beam Width (HPBW) is 27 degrees. The plot showed a HPBW(from Figure 5.3.1) of approximately 30° with an associated error due to the accuracy of the scale of $\pm 4^{\circ}$.

Observations were obtained twice daily. The equipment was turned on half an hour before the observation of the sun to allow it to stabilize. A series of scans was performed by rotating the antenna through the sun in azimuth once the altitude had been set for maximum signal input. The final output chart looked similar to that shown in Figure 5.3.2.a.This figure shows receiver output while observing the sun (in arbitrary units), as the antenna was turned through it. In each observing session a signal generator was used to calibrate the output voltage, as shown in Figure 5.3.2.b. The calibration was taken immediately after each observation.

5.4 Data Reduction

The data, as seen in Table I, were reduced as follows:

1. The time of the observation was recorded; 10:00 in the morning ADT(10M);3:00 in the afternoon ADT(3A).

2. The date was recorded.

3. The weather was recorded: sunny(S); cloudy(C); rain(R).

Calibration:

1. The number of units on the output chart paper were

Figure 5.3.1

Beam pattern of the one meter telescope as built up
by intensity scans of the sun. The intensity is in
arbitrary units normalized to one, while the azimuth
angle is in degrees. An uncertainty of $\pm 4^{\circ}$ is associated
with the measurements.
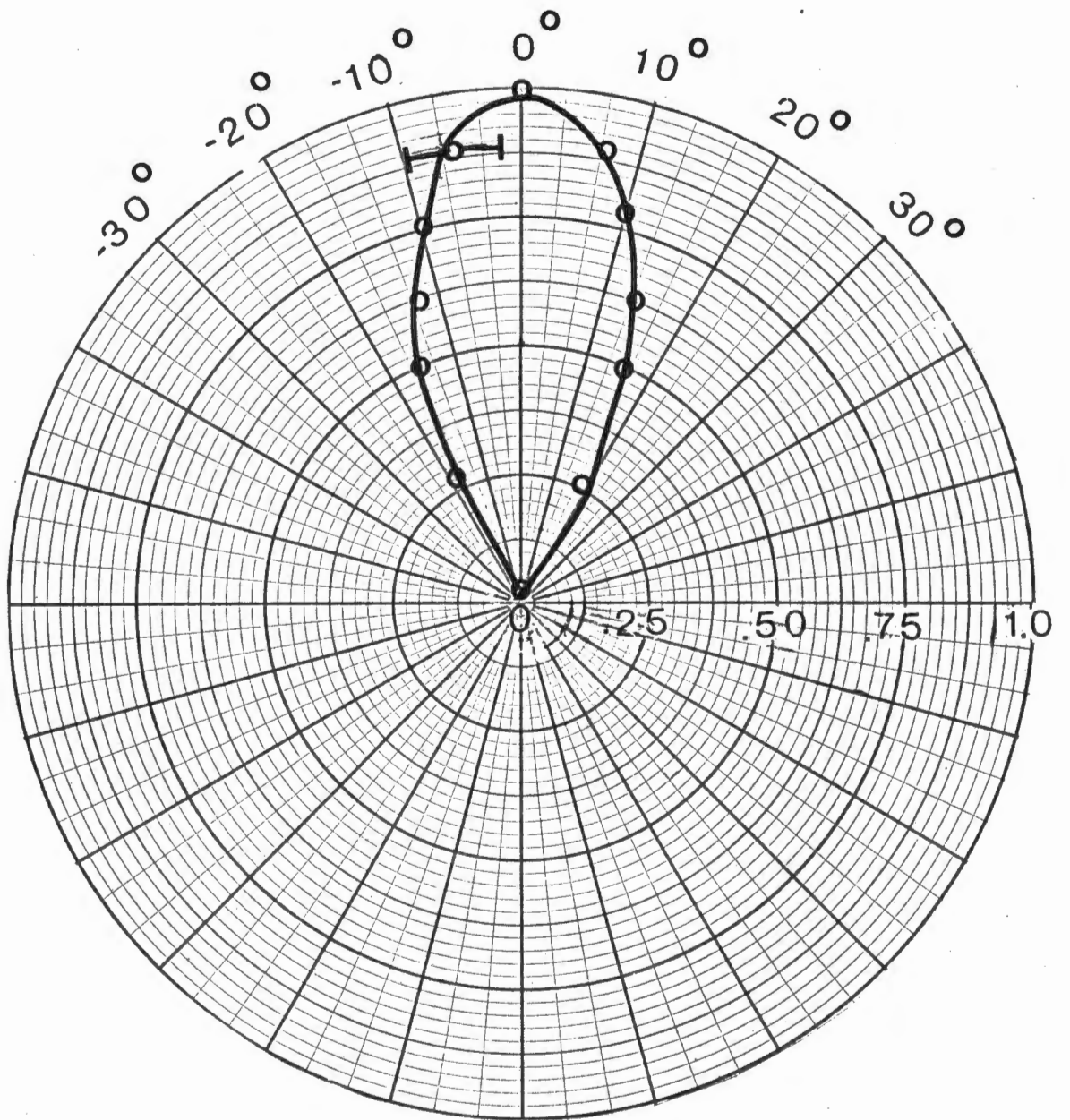
NORMALIZED

INTENSITY

Figure 5.3.2.a

Output from chart recorder for a single observing
session as telescope was scanned through the sun
several times. The encircled numbers indicated the
number of units of the peak from the baseline level.
Each set of observations took about five minutes.
Three scans were averaged to obtain $\bar{x}_{sun}$ for each
observing run.

Figure 5.3.2.b

Output from chart recorder for the signal generator
(Type 1021-A) showing the calibration voltages. The
encircled numbers indicate the number of units of the
peak from the baseline level. The baseline level changed
slightly due to the temperature instability of the
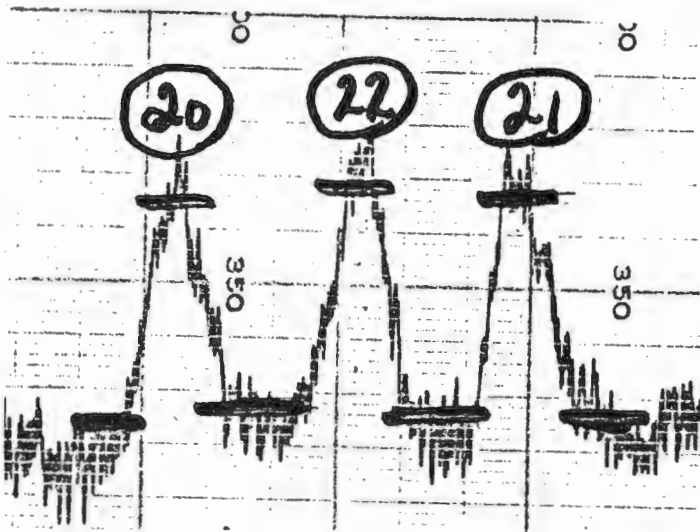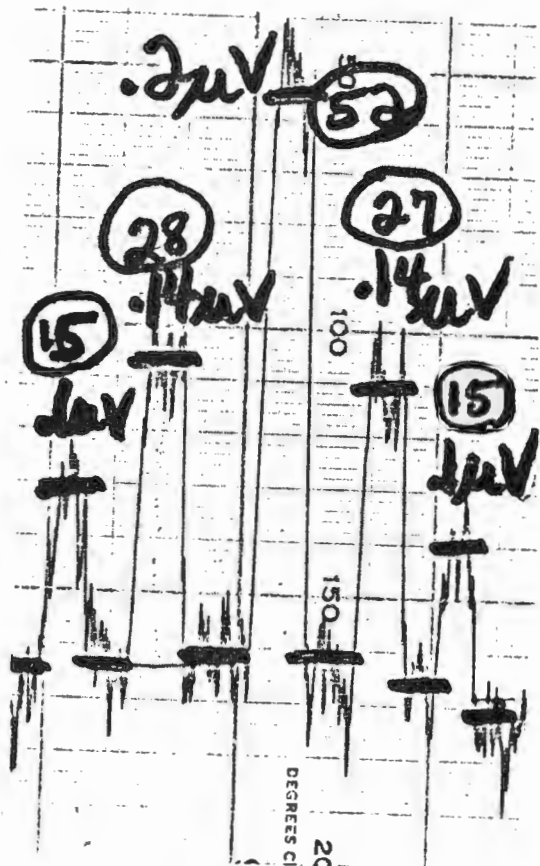receiver which caused a drift on the chart recorder.

FIGURE 5.3.2.a

FIGURE 5.3.2.b

counted for each of the generator signal outputs. The
noise level was averaged at the baseline and at the
-peak intensity points by eye. The units were then counted
for $0.1 \mu V$, $0.14 \mu V$, and $0.20 \mu V$ for the first 19
observations. These appear in the data table as $X_{0.10}$,
$X_{0.14}$, and $X_{0.20}$. For the last 7 observations a larger
number of calibration points were used so a better fit
of the data could be established. They appear in the data
table as $X_{0.10}$, $X_{0.12}$, $X_{0.14}$, $X_{0.16}$, $X_{0.18}$, $X_{0.20}$.
2. These last 7 observations, with 6 calibration points
each, were then used to transform from chart reading
to a signal voltage in microvolts. A linear least squares
fit was attempted, but this procedure was rejected in
favor of a freehand curve which fit the data more
precisely. (See Figure 5.3.3).
3. Three intensity scans of the sun were averaged for
each observation and the mean value labelled $\bar{x}_{sun}$ in
Table I.
4. The quantity $\bar{x}_{sun}$ was transformed to microvolts (μV)
using the calibration curve shown in Figure 5.3.3. Hence
for each value of $\bar{x}_{sun}$ a value of Y_{sun} could be obtained.
A sliding fit of the calibration curve was used for the
first 19 observations to give an accurate transformation
to obtain Y_{sun}.
5. There are two sources of error in Y_{sun}. First, an
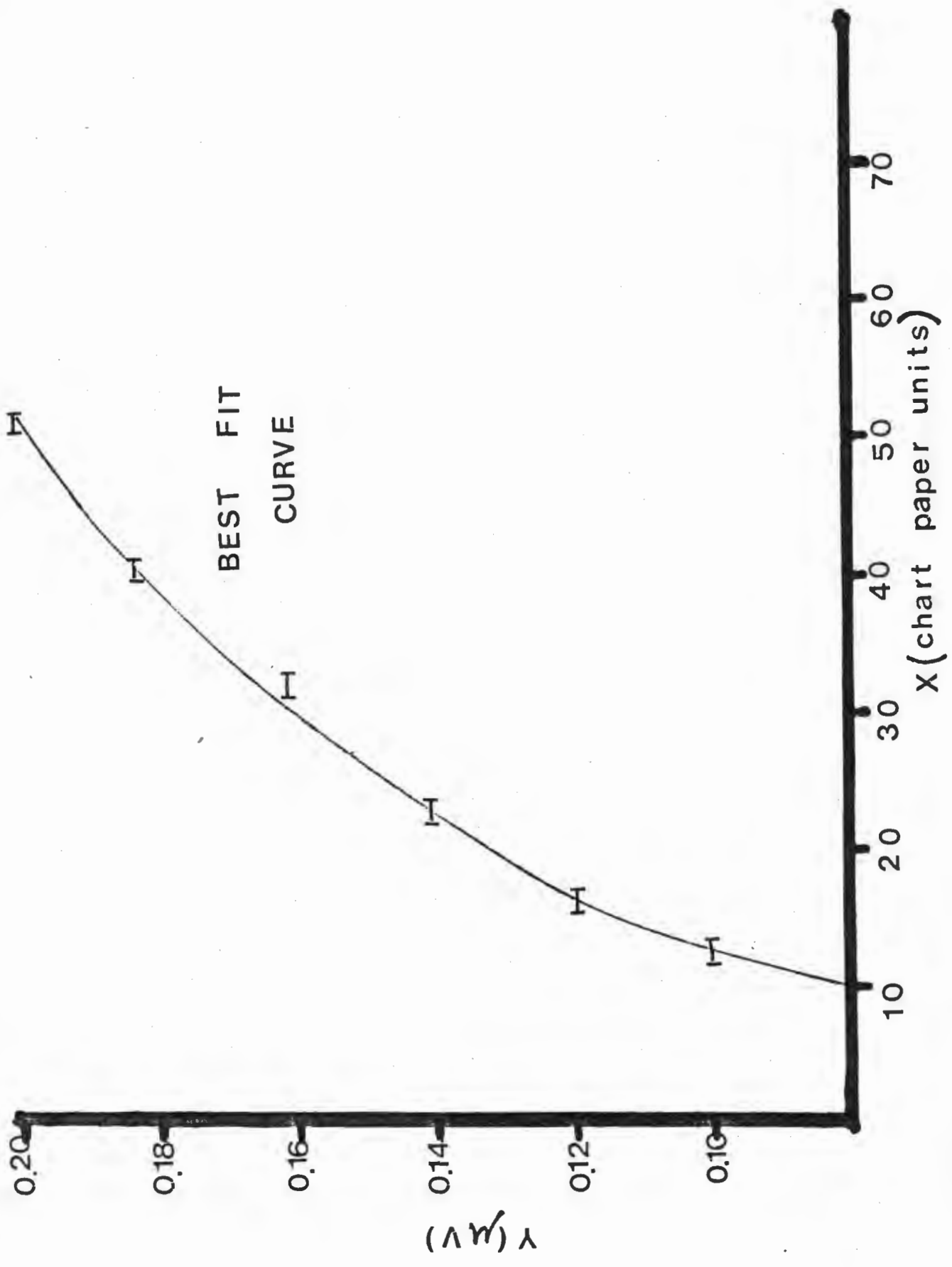error occurs due to the reading uncertainty from the

Table I

Observation	Time	Date	Weather	$X_{0.10}$	$X_{0.14}$	$X_{0.20}$	$\bar{x}_{sun}$	Y_{sun}	$S \cdot 10^{-22} Wm^{-2} Hz^{-1}$
1	10M	June20	C	12	18	45	15	.14	1.6
2	3A	20	S	12	18	45	15	.14	1.6
3	10M	21	C	12	18	44	18	.14	1.6
4	3A	21	S	12	20	43	22	.14	1.6
5	10M	22	C	13	23	43	28	.15	1.8
6	3A	22	C	11	19	42	24	.15	1.8
7	10M	23	C	12	22	45	22	.14	1.6
8	3A	23	S	13	21	43	23	.14	1.6
9	10M	24	S	12	18	41	20	.14	1.6
10	3A	24	S	11	21	44	19	.14	1.6
11	10M	25	S	13	21	42	22	.14	1.6
12	3A	25	C	12	22	42	23	.14	1.6
13	10M	27	C	15	28	52	27	.14	1.6
14	3A	27	C	15	28	52	27	.14	1.6
15	10M	28	C	13	27	50	23	.14	1.6
16	3A	28	S	13	24	49	28	.14	1.6

Observation	Time	Date	Weather	$X_{0.10}$	$X_{0.14}$	$X_{0.20}$	$\bar{x}_{sun}$	Y_{sun}	$S \cdot 10^{-22} {}_{Wm^{-2}Hz^{-1}}$
17	10M	29	C	15	25	55	28	.14	1.6
18	3A	29	C	12	25	50	25	.14	1.6
19	9M	30	S	13	22	52	27	.15	1.8

Observation	Time	Date	Weather	$X_{0.10}$	$X_{0.12}$	$X_{0.14}$	$X_{0.16}$	$X_{0.18}$	$X_{0.20}$	$\bar{x}_{sun}$	Y_{sun}	$S \cdot 10^{-22} {}_{Wm^{-2}Hz^{-1}}$
20	11M	30	S	12	18	23	32	38	52	27	.15	1.8
21	3A	30	S	12	17	24	33	40	50	27	.15	1.8
22	9M	Jy 1	R	12	16	22	32	37	49	23	.14	1.6
23	11M	1	R	12	16	23	34	38	51	23	.14	1.6
24	9M	2	C	13	16	25	33	39	53	25	.15	1.8
25	11M	2	C	13	16	25	34	39	53	25	.15	1.8
26	3A	2	C	11	15	23	32	38	52	25	.15	1.8

Figure 5.3.3

The freehand curve fit used to calculate Y_{sun}, given $\bar{x}sun$. The plot is the generator test voltages(Y) versus the number of units on the chart paper X. The error bars denote the standard deviation in the data at each Y test voltage.

BEST FIT
CURVE

X(chart paper units)

Y(μv)

output chart. This was estimated to be $\pm$ 2 units. The second is the uncertainty in fitting the data. The error due to the reading uncertainty is $\pm$.008μV. The error due to the fitting procedure is $\pm$.002μV, based on the free-hand fit of the curve. This gives a total error in Y_{sun} of $\pm$ .008μV.

6. Y_{sun} was then plotted versus the time of the observation. This is shown in Figure 5.4.3.

7. Next, the solar flux density was deduced from the formula:

$$S = \frac{V^2}{\Delta B A R \times efficiency}$$

where $V = Y_{sun}$

ΔB = bandpass

A = collecting area of the antenna

R = impedence of the line

The total error in S is due to the error in Y_{sun} of $\pm$ .008μV, the error in Δ B of $\pm$0.2 MHz, and the error in R of $\pm$ 5 ohms. This leads to an error in S of $\pm$0.50x10^{-22} Wm^{-2}Hz^{-1}. The solar flux density was then plotted on the right hand axis of Figure 5.4.3.

Figure 5.4.3

Plot of Y_{sun} versus time of observations for the 1m observing run. The flux density is also plotted on the right hand Y axis. Each time marking indicates 0^h ADT on the date of observation from June 20 to July 2. The error bar indicates an error in flux density of $\pm 0.5 \times 10^{-22} Wm^{-2}Hz^{-1}$
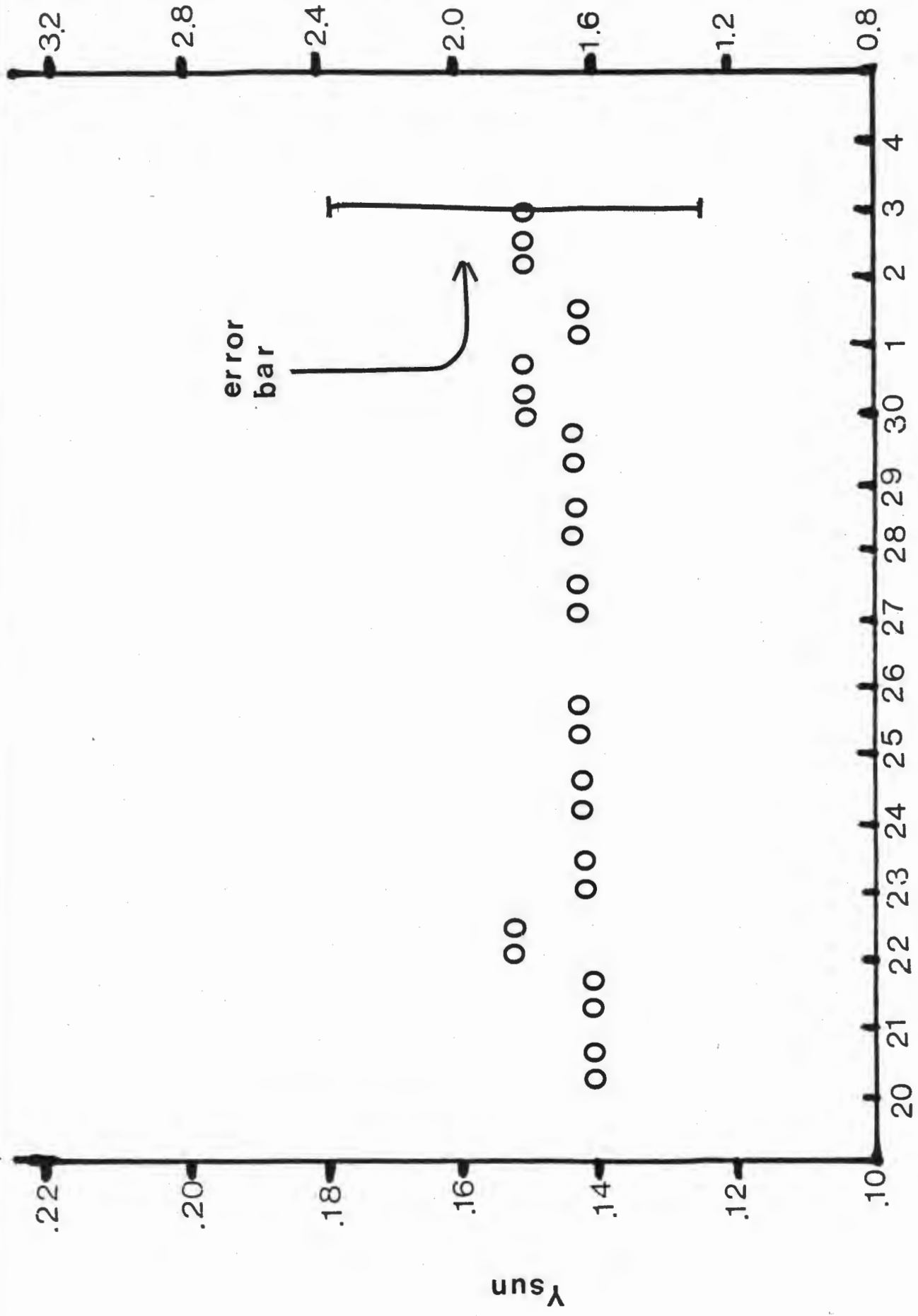
CHAPTER VI

SUMMARY AND CONCLUSIONS

After studying the data it may be concluded that the one
meter flux from the sun remained virtually constant (Figure
5.4.3) to within the uncertainties in the observations.
Unlike the solar flux at centimeter wavelengths, the one
meter observations produced flux densities comparable to
those expected for quiet sun levels. This could be due to
the fact that the source of 1m radio emission presumably
originates at a different height in the solar atmosphere.
In summary, future observations show promise of useful
results at both 3 cm and 1 m. The problems encountered
at 3 cm might still be a major task to overcome. The
alignment of the feed on the geometrical axis of the an-
tenna is very critical. The accurate alignment of the
antennas on the baseline, as well as the pointing accuracy,
will determine the success of receiving an interference
pattern. The receiver would have to be sensitive to the
expected flux levels.

The 3 cm project will be of more interest to astronomy
students because of its ability to resolve radio features
on the sun's disk. With the 16.8 m separation the 1 m
interferometer will not have sufficient resolving power to
accomplish this.

To facilitate useful interferometric observations

at 3cm from the sun the following recommondations are made:

1. a Dicke switch to improve the sensitivity and drift characteristics of the system;

2. a phase shifter to improve the symmetry;

3. thermal isolation of the electronics to eliminate the drift in the system;

4. a stable equatorial mounting capable of tracking the sun for an extended period of time;

5. a detailed study of horn alignment tolerances and their effect on overall sensitivity of the system.
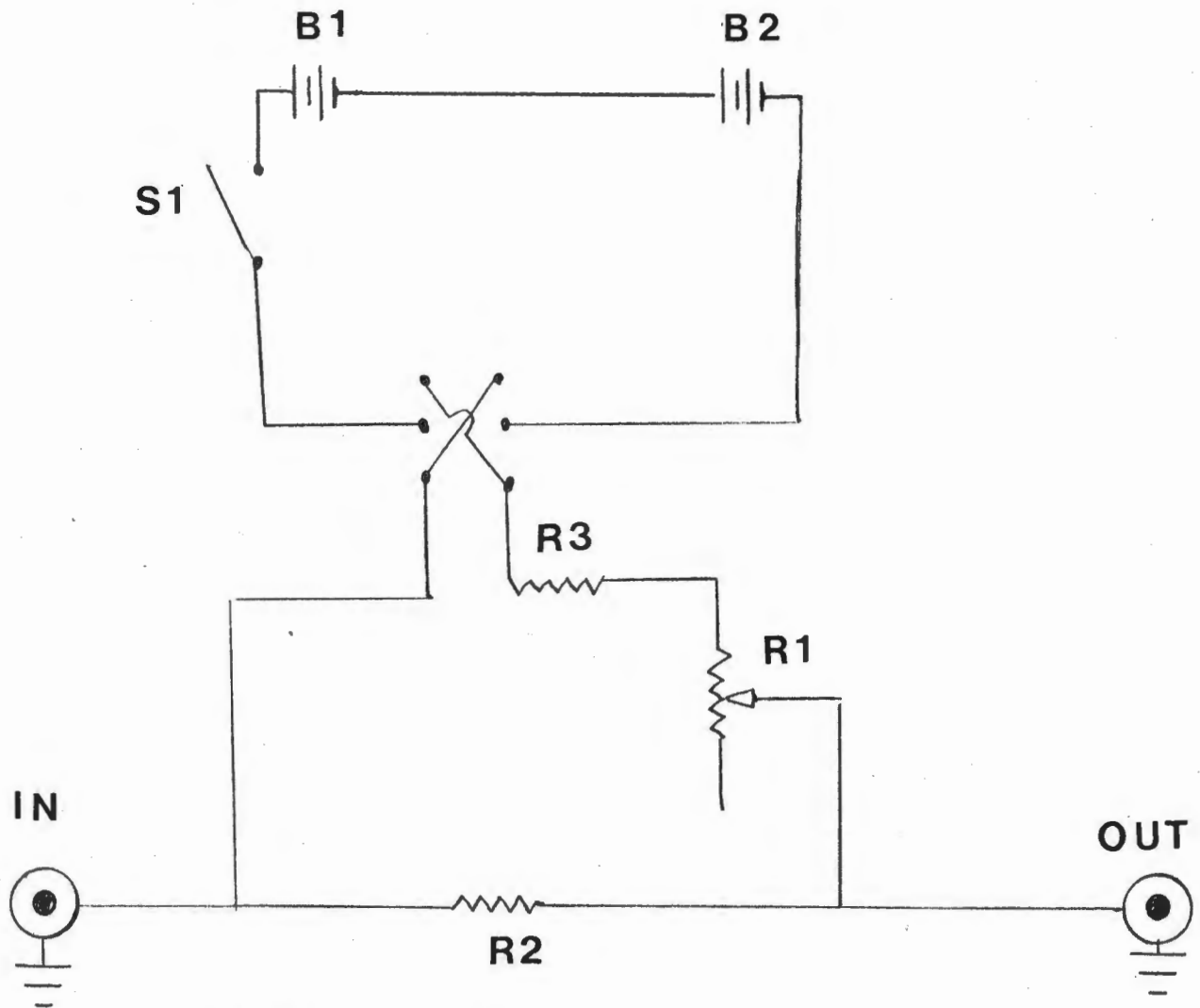
Appendix A

Basic Electronics (Schematics)

IF Stage:
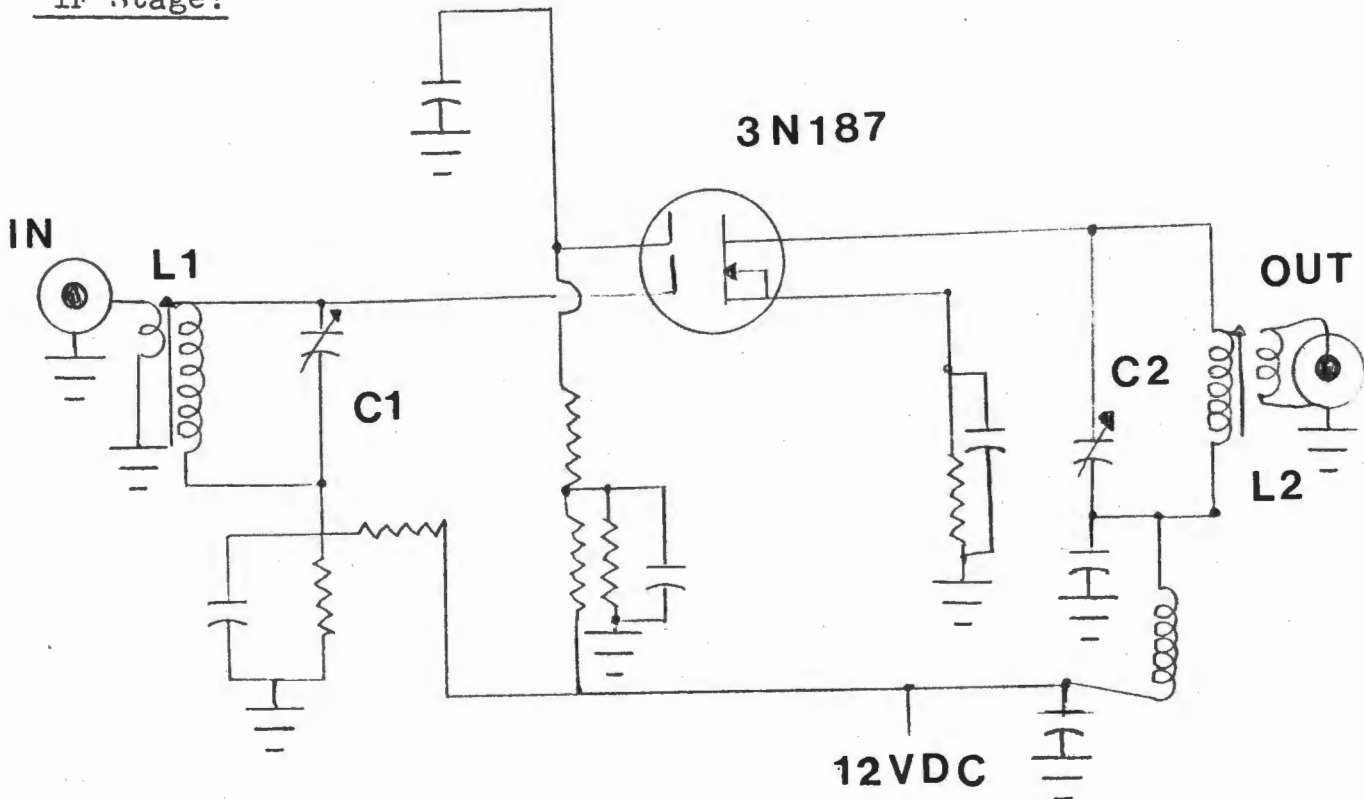
Typical IF Stage (adapted from RCA Transistor,
Thyristor and Diode Manual (1971), p.706)
L1, C1 and L2, C2 are resonant circuits which
are tuned to produce the desired bandpass
characteristics of the receiver.

Offset Unit :

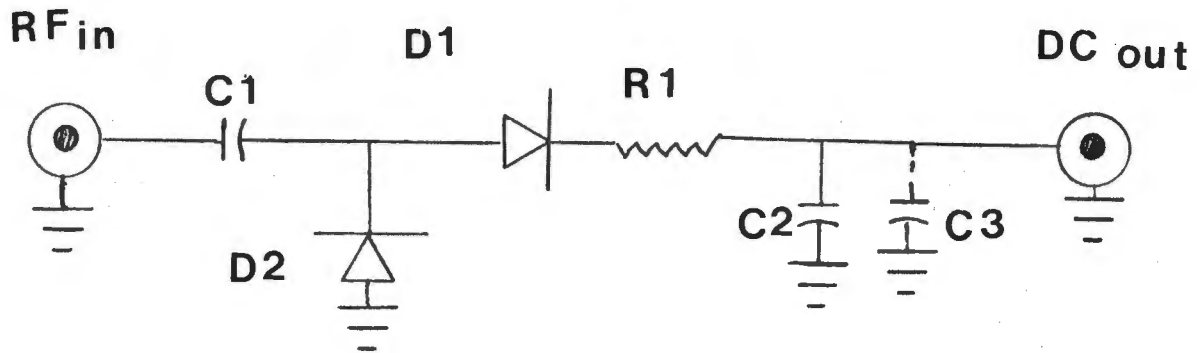**B1** **B2**

S1

R3

R1

IN **OUT**

R2

Offset Unit symbols :

```
     S1 - on-off switch
     S2 - polarity reversing switch
B1, B2 - 8.4 volt mercury cells (Mallory TR-126)
     R1 - 50K ten-turn potentiometer
     R2 - 200 ohm, ½w
     R3 - 10K, ½w
```

Demodulator Circuit :

Symbols :

D1, D2	-	1N34 (Germainium, point contact diodes)
R1	-	50K, $\frac{1}{4}$w
C1	-	100 pf
C2	-	100 pf
C3	-	cable capacitance

Appendix B

Test Equipment Specifications

I   Canadian Forces Test Signal Generator Model
TS-147B/UP

   (a) Frequency meter .

      (1) Range :   8500 MHz to 9600 MHz

      (2) Absolute Accuracy : $\pm$ 2.5 MHz at 25°C
and 60% relative humidity.

   (b) Power meter (output test signals)

      (1) Range :   - 42 to - 85 dBm at RF receptacle

      (2) Accuracy : $\pm$ 1.5 dB

II General Radio Company Type 1021-AU-UHF Test
Signal Generator.

   (a) Carrier frequency :

      (1) Range :   250 MHz to 920 MHz in one band

      (2) Accuracy : $\pm$ 1%

   (b) Output voltage .

      (1) Adjustable from 0.5 μV to 1.0V, open circuit.

      (2) Accuracy : $\pm$ 10%

III HP-430B Power meter

      (1) Power range :   .1-10.0 mw

      (2) Accuracy : $\pm$ 5% of full scale

IV Telonic Model 1205A Sweep Generator

      (1) Frequency range :   Band 1-(1-500 MHz)

      (2) Sweep width :   (200 KHz-500 MHz)

(3) RF output level = 0.5 Vrms

(4) Accuracy on frequency dial : $\pm$ 10 MHz

V   HP - 8601A Sweep Generator

  (a) Frequency Characteristics :

    (1) High frequency range 1-110 MHz

    (2) Accuracy : $\pm$ 1% of frequency

  (b) Output RF Characteristics :

    (1) Level : +20 to -110 dBm

    (2) Accuracy : $\pm$ 1dB

VI Tektronix RM503 Oscilloscope :

    (1) Sweep rate : 21 calibrated rates from
        1 μ sec/cm to 5 sec/cm.

    (2) Accuracy : $\pm$ 1% of the sweep rate

Appendix C

Additional Observations Using the

One Meter Interferometer

We now discuss some supplementary observations made using the 1m receiver along with the two-element inter-ferometer. The purpose was to observe the sun for several days and verify the temporal occurance of interference maxima and minima as well as their relative strengths.

Based on theory pertaining to a two-element inter-ferometer, the observed times for maxima and minima follow from the formulaes(Steinberg and Lequeux,1963):

$$t_M = \text{time of n-th maxima} = \sin^{-1}\frac{n\lambda}{L} \times 4\text{minutes}$$

$$t_m = \text{time of n-th minima} = \sin^{-1}\frac{(n+\frac{1}{2})\lambda}{L} \times 4\text{minutes}$$

λ = wavelength of observation=1.14m

n = n-th order term (i.e.,n=0,1,2,3,4,5,......)

L= length of baseline=16.8m

Based on these formulae and the fact that transit occured at about 1:10 ADT on July 3-5, times were pre-dicted for maxima and minima fringe amplitudes and these predicted times, along with averaged maxima and minima for three days observations, are shown in Table II.

From the comparison of maxima and minima it was concluded that the points lie close to the expected

data points. The errors in the times are most likely
due to the slight differences in cable length from the
antennas, and the azimuthal location of the antennas with
respect to North and South. One antenna was inadvertently
pointed slightly east of south about 2°, thus contributing
to a phase shift. A typical scan , using the 1m inter-
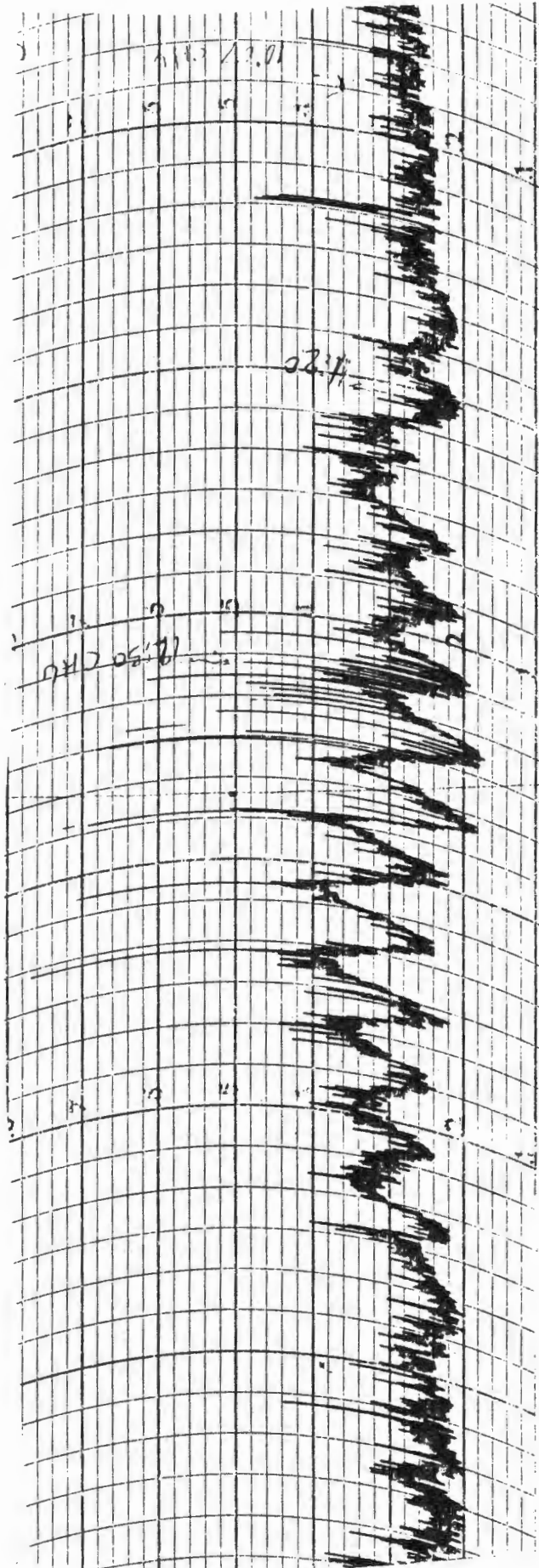ferometer is shown in Figure AI.

Table II

Expected Maxima	Observed Maxima[*]
12:38	12:33
12:54	12:49
1:10	1:03
1:26	1:24
1:42	1:42
1:58	1:58
2:14	2:13

Expected Minima	Observed Minima[*]
12:46	12:46
1:02	12:58
1:18	1:16
1:34	1:32
1:50	1:50
2:06	2:06

[*] Averaged results for three days.

Figure AI

Typical scan of the sun using the 1m interferometer.

TIME

REFERENCES

Adams, S.F. 1969, <u>Microwave Theory and Applications</u>

      (Englewood Cliffs, New Jersey : Prentice Hall, Inc.)

Allen, C.W. 1973, <u>Astrophysical Quantities, Third Edition</u>

      (London : The Athlone Press)

Christiansen, W.N. and Hogbom, J.A. 1969, <u>Radiotelescopes</u>

      (Cambridge : Cambridge University Press)

DeFrance, J.J. 1966, <u>Communications Electronics Circuits</u>

      (New York : Holt, Rinehart and Winston, Inc.)

Gibson, E.G. 1973, <u>The Quiet Sun</u>, (Washington : U.S.

      Government Printing Office)

Kakiniuma, T. and Swarup, G. 1962, "A Model for the Sources

      of the Slowly Varying Component of Microwave Solar

      Radiation." Ap. J., <u>136</u>, 975.

Kraus, J.D. 1966, <u>Radio Astronomy</u>, (New York : McGraw-Hill

      Book Company)

Steinberg, J.L. and Lequeux, J. 1963, <u>Radio Astronomy</u>,

      New York : McGraw-Hill Book Company)

Silver, S. 1964, <u>Microwave Antenna Theory and Design</u>

      (Boston : Boston Technical Publishers, Inc.)

Wolf, S. 1973, <u>Guide to Electronic Measurements and Laboratory</u>

      <u>Practice</u>, (Englewood Cliffs, N.J. : Prentice Hall, Inc.)